Optics & Laser Technology 167 (2023) 109681

Contents lists available at ScienceDirect

Optics and Laser Technology

journal homepage: www.elsevier.com/locate/optlastec

Full length article

An improvement to the infinite integration method Based on quadrant detector

Qian Li [a,d], Jiabin Wu [b], Huaming Yu [c,d], Xiaoning Luan [a,d], Fupeng Wang [a,d], Qingsheng Xue [a,d,*]

[a] College of Information Science and Engineering, Ocean University of China, Qingdao, Shandong 266100, China
[b] Changchun Institute of Optics, Fine Mechanics and Physics, Chinese Academy of Sciences, Changchun, Jilin 130033, China
[c] College of Oceanic and Atmospheric Sciences, Ocean University of China, Qingdao, Shandong 266100, China
[d] Engineering Research Center of Advanced Marine Physical Instruments and Equipment, Ministry of Education, China

ARTICLE INFO

Keywords:
Spot-positioning algorithm
Spot-positioning errors
Quadrant detector
Infinite integral method
Luminous energy

ABSTRACT

In this study, we propose a new method to improve the position measurement accuracy of the traditional infinite integral method (IIM) based on a quadrant detector (QD). First, the error source of the IIM is analysed in depth. Then, the influence of the detector size and gap width was considered to obtain a modified integration area. Thus, a new analytical expression was obtained. We performed several sets of simulations to test the validity of our proposed method, and the root-mean-square errors under different radii were all less than $5 \times 10^{-5} mm$. The experimental results show that when compared to IIM and the calibrated infinite integral method (CIIM), our novel method reduces error by 98.1% and 85.3%, respectively. One of the advantages of this technique is its simplicity; it requires fewer parameters and does not require pre-calibration compared with the fitting method. Therefore, this technique has the potential to be employed in space laser communication systems, optical tweezers, and precision measurements.

1. Introduction

Research on the laser-illuminated object position or precise determination of the laser beam position has a long history [1]. Compared with position-sensitive detectors (PSD) and charge-coupled devices (CCD), quadrant detectors (QD) [2–4] offer the advantages of high position resolution, a simple processing circuit, small junction capacitance, and a short response time[5–9]. They are commonly used in laser tracking and positioning [10–12], free-space optical communications [13], laser-guided weapons[14], and optical tweezers[15]. Nevertheless, because of the gap (also known as the blind area) between quadrants and the intensity distribution of the beam, there is usually a complex nonlinear relationship between the detector output signal and the actual position of the spot centroid, which seems to be a common problem [16–17].

Many spot-positioning algorithms have been developed over the last few decades to overcome this problem. Narag et al. proposed a new expression for the response of a QD using convolution integrals [18]. To enhance linearity, Cui et al. developed a new solution equation [19,20]. Based on mathematical physics equations, Wujie et al. built a virtual movement scheme to achieve better measurement accuracy [21]. Moreover, numerous recent studies [22–24] have demonstrated that backpropagation (BP) neural networks are also a viable approach. However, these studies were relatively complex and time consuming. An alternative approach to the problem is the fitting method [25–28], the central issue of which is to use various types of functions to fit the nonlinear relationship. By ignoring the influence of the detector size and gap, IIM obtains the approximate position of the spot centroid in the form of an error function. However, IIM suffers from low accuracy [29]. Wu et al. further showed that by introducing an error compensation factor, the CIIM proposed using least-squares fitting can effectively improve the accuracy of the IIM [30–32]. However, these studies have certain drawbacks. First, a large amount of data needs to be collected in advance for calibration or training; second, they are multi-parameter, and the increasing number of calculations limits their application.

This study examines some previous works and proposes a novel algorithm capable of theoretically eliminating two kinds of errors originating from detector size and gap width. These errors are deeply analysed, and a new formula is proposed to compensate for the inherent defects of the IIM, resulting in better accuracy. Another advantage of this method is that there is no need for pre-calibration, which makes it more practical.

* Corresponding author.
E-mail address: xueqingsheng@ouc.edu.cn (Q. Xue).

https://doi.org/10.1016/j.optlastec.2023.109681
Received 2 July 2022; Received in revised form 19 November 2022; Accepted 31 May 2023
Available online 13 June 2023

The rest of the paper is organised as follows. We start our paper by presenting the principle of the QD in Section 2.1. In Section 2.2, both IIM and CIIM are described, and the limitations of IIM are briefly discussed. A new method is proposed in Section 2.3. We also experimentally demonstrate the feasibility of the new method under different radii in Section 3. Finally, conclusions are presented in Section 4.

2. Methodology

2.1. Principle of the QD

Our theory is based on the assumption that the spot energy distribution of the laser can be approximated using a Gaussian distribution [33]:

$$D(x,y)=\frac{2P_0}{\pi\omega^2}exp\left(-2\frac{(x-x_0)^2+(y-y_0)^2}{\omega^2}\right), \tag{1}$$

where P_0 is the total energy of the Gaussian beam, ω the radius of the spot, and (x_0,y_0) the position of the spot centroid.

A QD is a device made of four identical photodiodes separated by small gaps that cause a loss of light energy [34]. When illuminated, four units can output photocurrent independently, and the amplitude of the photocurrent in each unit $I_{Ai},I_{Bi},I_{Ci},I_{Di}$ is proportional to the spot energy incident on the unit [4]:

$$I_i\propto\iint_{S_i}D(x,y)dxdy(i=A,B,C,D). \tag{2}$$

As shown in Fig. 1, when the spot centroid is at the centre of the QD, the amplitude of the output photocurrent of the four units is equal. As the spot centroid deviates from the centre, the balance is broken. The position of the spot centroid can be determined according to this principle.

The detection process for the spot position of the QD can be abstracted and simplified into a diagram (Fig. 2). First, the solution values of the x-axis and y-axis are calculated according to rules f:

$$E_X=f_X(I_A,I_B,I_C,I_D)=\frac{(I_A+I_D)-(I_B+I_C)}{I_A+I_B+I_C+I_D}, \tag{3}$$

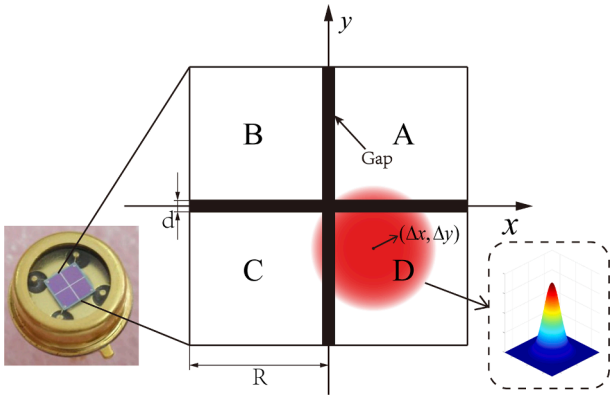

Fig. 1. Spot position detection of the QD.

$$E_Y=f_Y(I_A,I_B,I_C,I_D)=\frac{(I_A+I_B)-(I_C+I_D)}{I_A+I_B+I_C+I_D}. \tag{4}$$

It can be seen that the solution value (E_X,E_Y) is a normalised value, which represents the offset degree of the spot relative to the centre of the QD. However, this does not mean that the position of the spot centroid is the value of the solution: $(x_0,y_0)\neq(E_X,E_Y)$. In fact, an S-shaped nonlinear relationship exists between the solution value and actual position [35]. To obtain the approximation of the spot centroid (x_0',y_0'), the spot position detection method h must be used. In addition, because the energy density distribution of the spot and the shape of the detector are symmetrical, the position relationship between the x- and y-axes is independent of each other. Thus, only the situation in the x-axis direction will be discussed later.

2.2. Infinite integral method (IIM)

As the laser is incident on the QD (the detector size is R and the gap width is d), the relationship between the solution value and the actual position of the spot centroid can be obtained as follows:

$$E_X=\frac{\left(\int_{-A}^{A}\int_{B}^{A}D(x,y)dxdy-\int_{-B}^{B}\int_{B}^{A}D(x,y)dxdy\right)-\left(\int_{-A}^{A}\int_{-A}^{-B}D(x,y)dxdy-\int_{-B}^{B}\int_{-A}^{-B}D(x,y)dxdy\right)}{\left(\int_{-A}^{A}\int_{B}^{A}D(x,y)dxdy-\int_{-B}^{B}\int_{B}^{A}D(x,y)dxdy\right)+\left(\int_{-A}^{A}\int_{-A}^{-B}D(x,y)dxdy-\int_{-B}^{B}\int_{-A}^{-B}D(x,y)dxdy\right)}, \tag{5}$$

where $A=R,B=d/2$. This is typically a complex problem with a transcendental equation that cannot be solved directly.

This problem is usually overcome by considering the detector size in (5) as infinity $(R\to\infty)$ and ignoring the influence of the gap $(d\to0)$, as follows:

$$E_X\approx\frac{\int_{-\infty}^{\infty}\int_{0}^{\infty}D(x,y)dxdy-\int_{-\infty}^{\infty}\int_{-\infty}^{0}D(x,y)dxdy}{\int_{-\infty}^{\infty}\int_{-\infty}^{\infty}D(x,y)dxdy}=erf\left(\frac{\sqrt{2}}{\omega}x_0'\right), \tag{6}$$

$$erf(x)=\frac{2}{\sqrt{\pi}}\int_0^x e^{-t^2}dt.$$

Finally, by taking the inverse function on both sides of the equal sign in (6), the IIM expression can be derived as follows:

$$x_0'\approx\frac{erf^{-1}(E_X)\cdot\omega}{\sqrt{2}}. \tag{7}$$

Unfortunately, when the spot centroid gradually moves away from the origin of the detector, the accuracy of IIM decreases significantly [29]. Assuming a spot with a radius of 0.85 mm is incident on the detector, the spot centroid moves in a fixed range[-0.5 mm,0.5 mm], the d is changed from 0 mm to 0.1 mm, and R is changed from 1 mm to 2 mm, and the root-mean-square error of the IIM is simulated by MATLAB 2022a, which is shown in Fig. 3 (the axes are normalised to the spot radius).

Based on the previous analysis, it can be concluded that the error should be proportional to d and inversely proportional to R, but some interesting phenomenon occurred: as d approached zero $(d\to0)$, the error was inversely proportional to R, which was in line with our expectations. However, as d increased, the situation began to reverse. This is due to the fact that the error caused by the d gradually plays a leading role. If the R is large enough, the error increases with the d, which is consistent with the results of previous studies. As R approaches the spot radius $(R\to\omega)$, the proportion of the error caused by R increases, and the total error first decreases and then increases as the d increases. As discussed, R and d play a major role in IIM error. Thus, these two factors

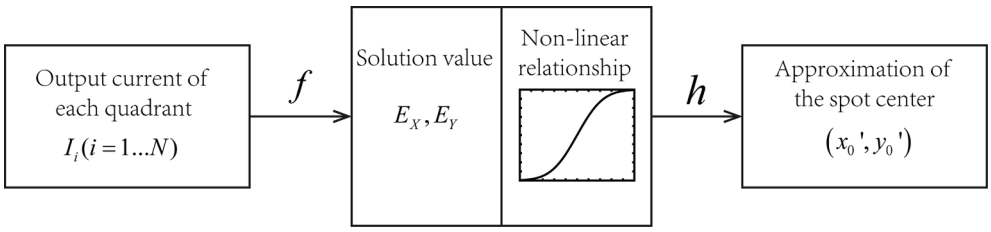

Fig. 2. Diagram of QD spot position detection.

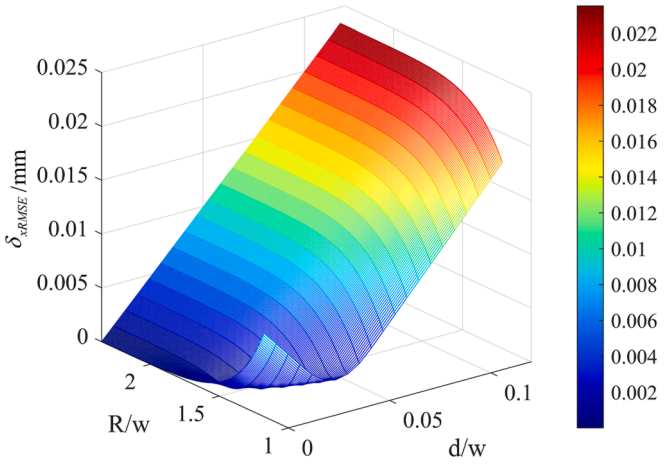

Fig. 3. The relationship between the root-mean-square error of the IIM with d/w and R/w.

deserve further attention.

The objective of the calibrated infinite integration method (CIIM) [32] is to further reduce the error of IIM, and an error compensation factor $\eta = f(\omega, R, d)$ is introduced in consideration of the error effects of the detector diameter and the gap size. The estimation of the beam position can be rewritten as follows:

$$x_0' = \frac{erf^{-1}(E_X)}{\sqrt{2}} \cdot \omega \cdot \eta(\omega, R, d), \tag{8}$$

where $\eta(\omega, R, d)$ introduces factors R and d that are not considered in the IIM. Because R and d are fixed in practical applications, the last two parameters can be combined into one, redefined as the effective beam radius $\omega_e = \omega \cdot \eta(\omega, R, d)$, then:

$$x_0' = \frac{erf^{-1}(E_X)}{\sqrt{2}} \cdot \omega_e. \tag{9}$$

With the least square method, N sets of experimental data $E_{X_n}(n = 1 \cdots N)$ were used for pre-calibration to obtain the optimal ω_e:

$$\omega_e = \frac{\sum_{n=1}^{N} m(E_{X_n}) \cdot x_n}{\sum_{n=1}^{N} m^2(E_{X_n})}, m(x) = \frac{erf^{-1}(x)}{\sqrt{2}}. \tag{10}$$

Obviously, CIIM requires a large amount of collected data in advance, which is impossible in some applications. In brief, there is an urgent need for a method with high precision, fewer parameters, and no need for pre-calibration.

2.3. Improved infinite integral method (IIIM)

To rectify these problems, the error source of the IIM was analysed in depth. Taking the calculation of the photocurrent of the two units on the right half as an example, the real value should be

$$I_R = I_A + I_D = \int_{-R}^{R}\int_{d/2}^{R} D(x,y)dxdy - \int_{-d/2}^{d/2}\int_{d/2}^{R} D(x,y)dxdy. \tag{11}$$

Using the IIM, we have:

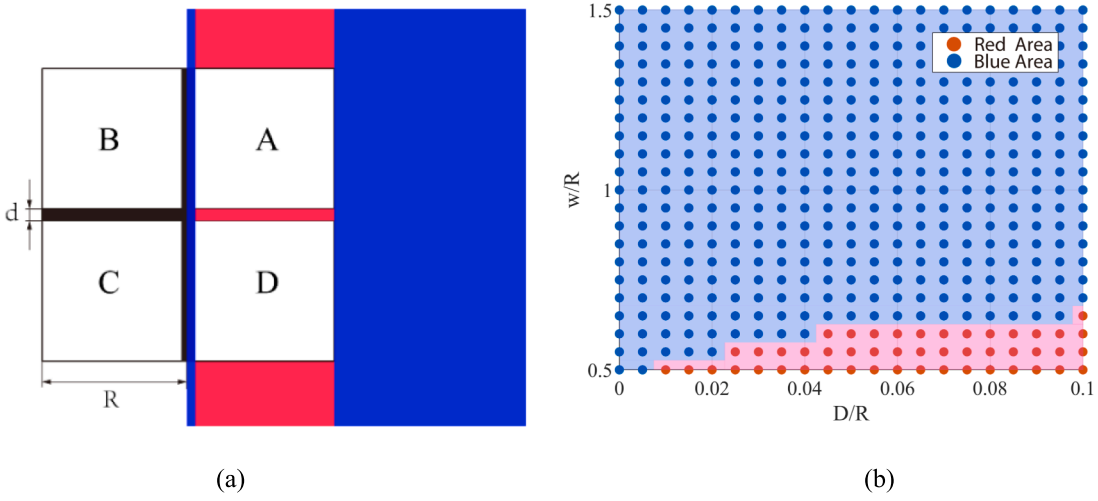

Fig. 4. (a)Diagram of the integration area of IIIM, the blue/red integration areas are redundant compared with the actual situation. (b)Comparison of the light energy of the red/blue areas (R=1mm, spot centroid moves in a fixed range[-0.5 mm,0.5 mm]). The region is coloured blue where the light energy of the blue area exceeds that of the red area; the remaining region is coloured red. (For interpretation of the references to colour in this figure legend, the reader is referred to the web version of this article.)

$$I_R = I_A + I_D \approx \int_0^{\infty}\int_0^{\infty} D(x,y)dxdy + \int_{-\infty}^{0}\int_0^{\infty} D(x,y)dxdy$$
$$= \int_{-\infty}^{\infty}\int_0^{\infty} D(x,y)dxdy. \quad (12)$$

To facilitate this demonstration, we analysed only the right half of the detector. As shown in Fig. 4(a), the error of the IIM originates from its integration area: the blue/red areas are redundant, which also means that the light energy calculated by the IIM is greater than the real value. Fig. 4(b) compares the light energy of the red/blue area with the changes in d/R and w/R. In most cases, the energy in the blue area exceeded that in the red area. If we remove the redundant blue area from the integral area of IIM, the following equation is obtained:

$$I_R \approx \int_{-\infty}^{\infty}\int_0^{\infty} D(x,y)dxdy - \int_{-\infty}^{\infty}\int_0^{d/2} D(x,y)dxdy - \int_{-\infty}^{\infty}\int_R^{\infty} D(x,y)dxdy$$
$$= \int_{-\infty}^{\infty}\int_{d/2}^{R} D(x,y)dxdy = erf\left[\frac{\sqrt{2}\,(x_0 - d/2)}{\omega}\right] - erf\left[\frac{\sqrt{2}\,(x_0 - R)}{\omega}\right]. \quad (13)$$

Similarly:

$$I_L = I_B + I_C \approx erf\left[\frac{\sqrt{2}\,(x_0 + R)}{\omega}\right] - erf\left[\frac{\sqrt{2}\,(x_0 + d/2)}{\omega}\right]. \quad (14)$$

Therefore, the new solution value can be expressed as:

$$E_X = T(x_0, \omega, d) = \frac{erf\left[\frac{\sqrt{2}\,(x_0-d/2)}{\omega}\right] - erf\left[\frac{\sqrt{2}\,(x_0-R)}{\omega}\right] - erf\left[\frac{\sqrt{2}\,(x_0+R)}{\omega}\right] + erf\left[\frac{\sqrt{2}\,(x_0+d/2)}{\omega}\right]}{erf\left[\frac{\sqrt{2}\,(x_0-d/2)}{\omega}\right] - erf\left[\frac{\sqrt{2}\,(x_0-R)}{\omega}\right] + erf\left[\frac{\sqrt{2}\,(x_0+R)}{\omega}\right] - erf\left[\frac{\sqrt{2}\,(x_0+d/2)}{\omega}\right]}. \quad (15)$$

When (ω, d) are determined, $T(x_0, \omega, d) \rightarrow T(x_0)$. The analytical formula of the IIIM is obtained:

$$x_0^{'} = T^{-1}(E_X) = G(E_X). \quad (16)$$

The maximum error δ_{xMAX} and root-mean-square error δ_{xRMSE} are adopted to evaluate the new method. δ_{xMAX} is the maximum value of $|\delta_i|$, which represents the extreme value of error in the detection range.

$$\delta_{xMAX} = MAX(|\delta_i|) = MAX(|x_{0i} - x_{0i}^{'}|). \quad (17)$$

δ_{xRMSE} is the root-mean-square error (RMSE), which is used to measure the deviation between the observed and actual values in the entire detection range:

$$\delta_{xRMSE} = \sqrt{\frac{1}{N}\sum_{i=1}^{N}\delta_i^{\,2}} = \sqrt{\frac{1}{N}\sum_{i=1}^{N}(x_{0i} - x_{0i}^{'})^2}. \quad (18)$$

Fig. 5(a) shows the errors of the three methods when $w = 0.85mm, R = 1mm, d = 0.3mm$. The δ_{xRMSE} of IIM, CIIM and IIIM are $5.12 \times 10^{-2}mm$, $4.20 \times 10^{-3}mm$ and $1.60 \times 10^{-5}mm$ respectively. Although the error of the CIIM is greatly reduced, there is still a certain gap compared with the IIIM.

In order to test the robustness of IIIM at different spot radii, the radius of the beam is changed from 0.75 mm to 1.05 mm. From the simulation results shown in Fig. 5(b), key findings emerge: Among the three methods, IIIM has the smallest δ_{xRMSE}, which is less than $5.0 \times 10^{-5}mm$ under different spot radii. Moreover, IIIM exhibits a minimum error when $w = 0.85mm$. We speculate that this might be due to the following reasons. Because a Gaussian beam with a smaller radius has a more concentrated energy distribution, most of the light energy falls into the gap (part of the red area), which leads to a decrease in accuracy. For a Gaussian beam with a radius much greater than approximately half the detector size, the main source of the error is the large amount of light energy falling outside (another part of the red area). As a result, the Gaussian beam with a radius of approximately 0.85 mm is less affected by the gap, while avoiding a large amount of energy loss outside.

Table 1 compares the δ_{xMAX} values of the three methods for different spot radii. Among the three methods, IIIM has the smallest δ_{xMAX}, which

Table 1
Comparison of δ_{xMAX} of three methods at different radii in simulation.

Method	ω/mm			
	0.75	0.85	0.95	1.05
IIM	$0.1114mm$	$8.42 \times 10^{-2}mm$	$3.85 \times 10^{-2}mm$	$1.82 \times 10^{-2}mm$
CIIM	$1.49 \times 10^{-2}mm$	$1.19 \times 10^{-2}mm$	$6.80 \times 10^{-3}mm$	$5.60 \times 10^{-3}mm$
IIIM	$4.17 \times 10^{-4}mm$	$8.22 \times 10^{-4}mm$	$5.47 \times 10^{-4}mm$	$4.31 \times 10^{-4}mm$

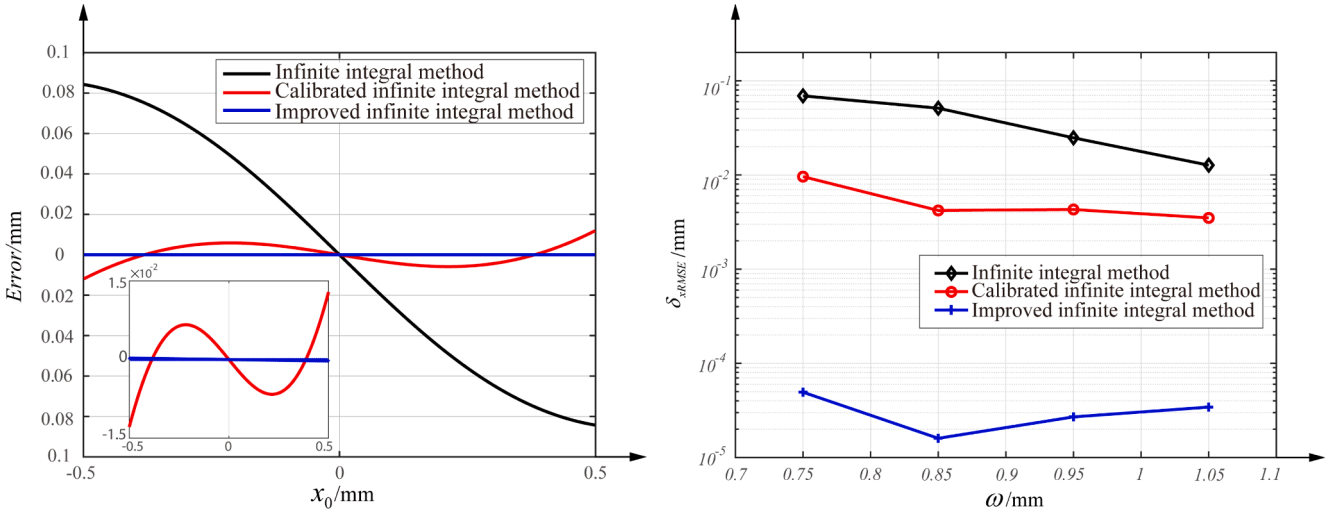

Fig. 5. (a)The simulation curves of positioning errors using three different methods ($w = 0.85mm$). (b)Comparison of δ_{xRMSE} between three different methods in simulation.

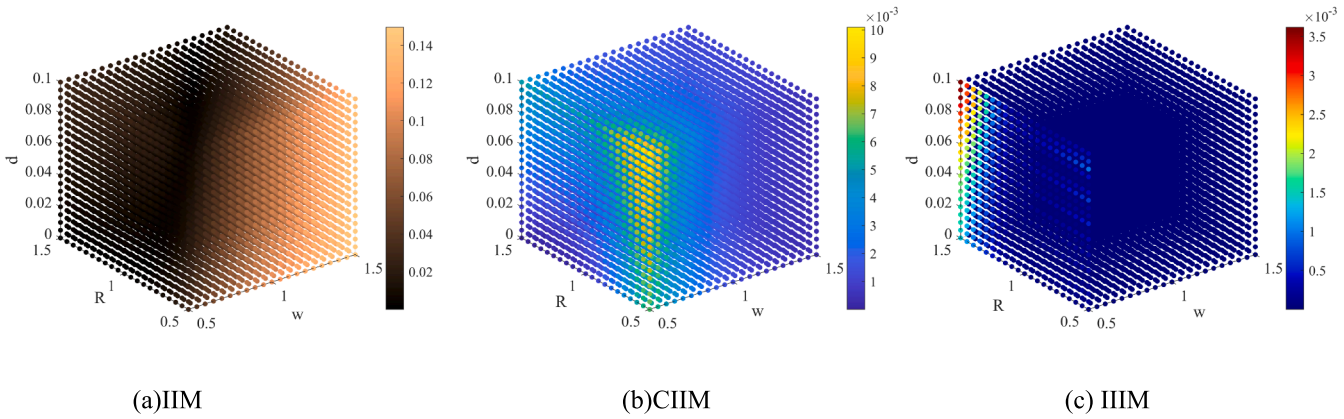

Fig. 6. Comparison of the δ_{xRMSE} between three methods in simulation.

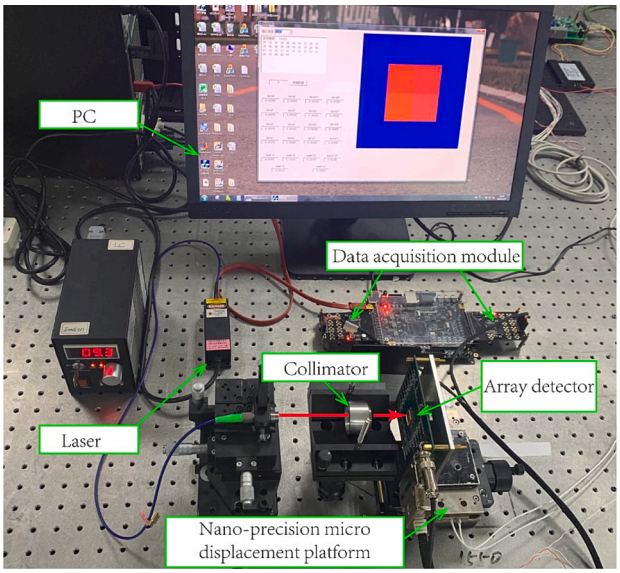

Fig. 7. Physical map of displacement test platform.

is less than $1 \times 10^{-3} mm$ under different spot radii.

Furthermore, the δ_{xRMSE} of IIM/CIIM/IIIM was simulated with different combinations of d, R, and ω (Fig. 6). It is evident that the δ_{xRMSE} of IIIM is significantly lower than that of the other two methods under different conditions.

In brief, the IIIM presented in this paper has a better performance both in terms of δ_{xMAX} and δ_{xRMSE}, and it also shows good robustness. The correctness of the IIIM was verified by the simulation results.

3. Experiment

3.1. Experiment setup

A displacement test platform, as shown in Fig. 7, was set up to verify the improvement in measurement accuracy of the IIIM. The light source was an 850 nm fibre laser (DL-850–030-T, SFOLT), whose optical power was continuously adjustable. The Gaussian beams emitted by the laser were changed into parallel beams by collimating and shaping lens groups and then focused on a QD array (mod1-25d, OTRON, $R = 1$ mm, and $d = 0.3$ mm) by a coupling lens (focal length:120 mm, self-made). As shown in Fig. 8, the detector was installed on a customised amplification circuit board (OPA2177, Analogue Devices) at a magnification of 10^6. It is important to note that because the research object of this study is QD, only four specific units are used. To achieve a high-precision displacement in the x-axis direction, the amplification circuit board is mounted on a one-dimensional displacement platform (n-644.3a, PI, positioning accuracy: 2 nm). The data acquisition module was a 16-channel simultaneous sampling data acquisition system equipped with two 16-bit SAR ADCs (AD7606,Analog Devices) and FPGA (EP4CE30F23C8).

The experimental procedure is as follows. First, the 850 nm laser is collimated and focused on the QD array through a coupling lens to form a spot with a radius of 0.85 mm. The spot was then moved from 0 mm to 0.5 mm at intervals of 0.005 mm using the one-dimensional nano-precision micro-displacement platform. The photocurrent was amplified and transmitted to a PC. The experiment was conducted in a dark room to reduce the influence of background noise. To verify the applicability of the new model at different radii, we varied the radius from 0.75 mm to 1.05 mm and repeated the above steps.

3.2. Results and analysis

Here, we compare the results of the proposed method with those of traditional methods in Fig. 9(a). The δ_{xMAX} of IIIM is $2.50 \times 10^{-3} mm$, which is 97.0% lower than that of IIM ($8.38 \times 10^{-2} mm$) and 80.8% lower than that of CIIM ($1.30 \times 10^{-2} mm$). Moreover, the δ_{xRMSE} of IIIM was $1.00 \times 10^{-3} mm$, which is approximately 1/50 of that of IIM ($5.18 \times 10^{-2} mm$) and 1/6 of that of CIIM ($6.80 \times 10^{-3} mm$).

As shown in Fig. 9(b), the accuracy of IIIM, which is higher than that of IIM and CIIM, shows good stability at various radii. The overall trend of the IIIM agreed well with the simulation results (Fig. 5(b)), whose δ_{xRMSE} at different relative beam radii were all less than $6 \times 10^{-3} mm$. Table 2 shows a comparison of the δ_{xMAX} values of the three methods for different beam radii. Among the three methods, the IIIM showed the smallest δ_{xMAX} for different beam radii.

The preceding analysis and discussion show that there is a disparity between the experimental and simulation results, which may be ascribed to ambient noise and will be the topic of our subsequent study. Nonetheless, the IIIM shows better accuracy in both δ_{xRMSE} and δ_{xMAX}, and it also exhibits a more stable measurement accuracy for different incident beam radii. The correctness of the IIIM was verified by the experimental results. It is worth noting that the new method not only has high accuracy but also does not need to be calibrated in advance.

4. Conclusion

In summary, a different approach to the traditional IIM problem is presented in this paper. By analysing the error source of the traditional IIM, a method to further improve its accuracy is found; that is, the light energy obtained by the detector is modified by removing the redundant integral area to compensate for the influence of the gap width and de-

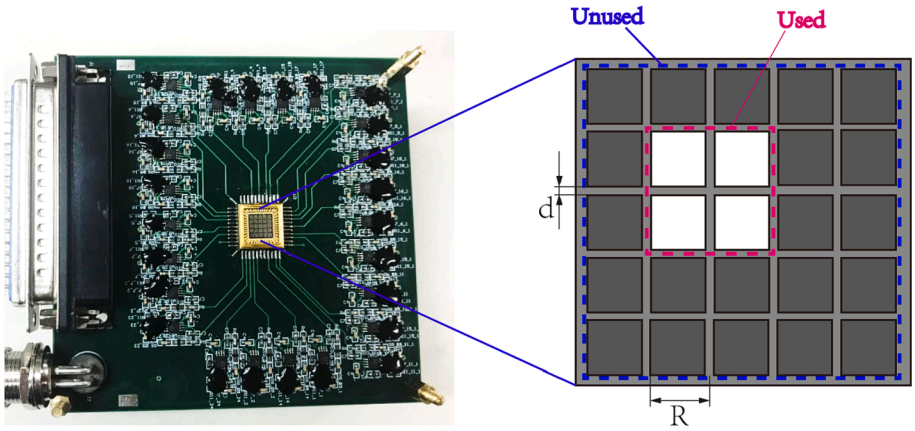

Fig.8. Physical map of QD array (mod1-25d, OTRON), only 4 specific units are used.

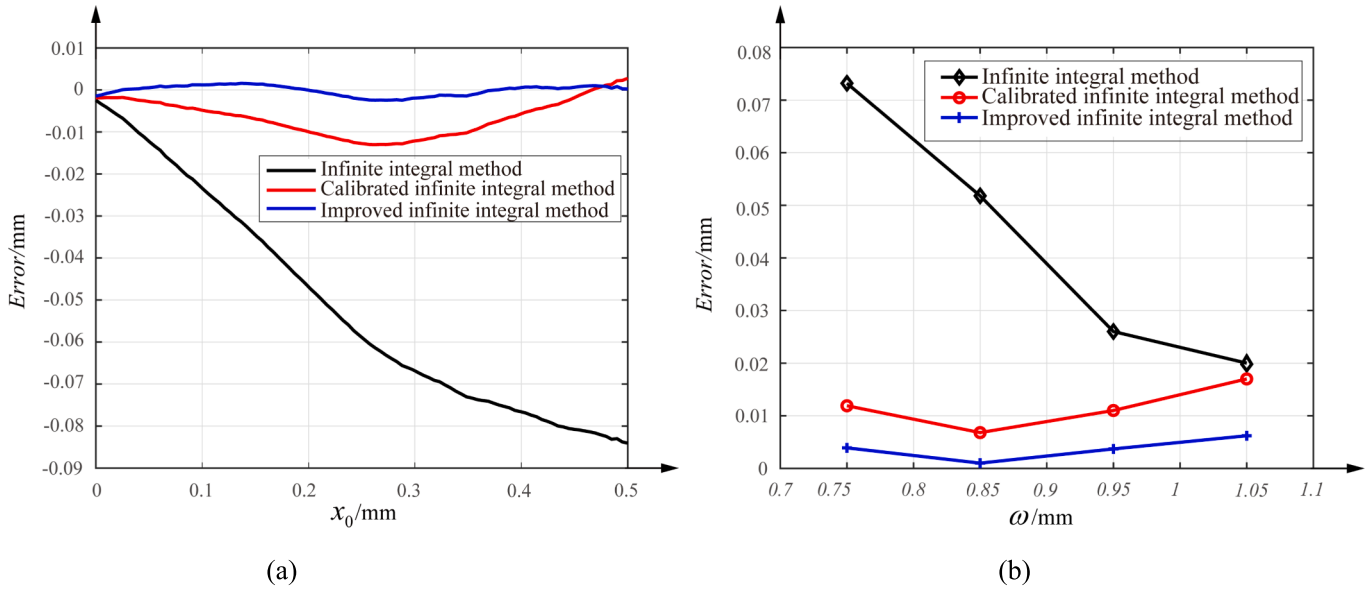

Fig. 9. (a). Experimental results of three methods ($w = 0.85mm$). The measurement range is from 0 mm to 0.5 mm for the symmetrical characteristic of position measurement errors. (b). The δ_{xRMSE} of three methods at different relative beam radii in experiment.

Table 2
Comparison of δ_{xMAX} of three methods at different radii in experiment.

Method	ω/mm			
	0.75	0.85	0.95	1.05
IIM	$0.1173mm$	$8.38\times10^{-2}mm$	$3.48\times10^{-2}mm$	$2.74\times10^{-2}mm$
CIIM	$1.59\times10^{-2}mm$	$1.30\times10^{-2}mm$	$1.61\times10^{-2}mm$	$2.72\times10^{-2}mm$
IIIM	$8.50\times10^{-3}mm$	$2.50\times10^{-3}mm$	$9.70\times10^{-3}mm$	$1.95\times10^{-2}mm$

tector size. When compared with fitting methods such as CIIM, IIIM has greatly improved accuracy and does not require pre-calibration because the error is corrected at the principle level. It is suitable for practical applications in which pre-calibration cannot be used. According to the experimental results, IIIM showed stability in both δ_{xRMSE} (all less than $6\times10^{-3}mm$) and δ_{xMAX} (all less than $2\times10^{-2}mm$) for different beam radii. In view of the above advantages, the IIIM is expected to be applied in the engineering practice of spot position measurements.

CRediT authorship contribution statement

Qian Li: Writing – original draft, Conceptualization, Methodology. **Jiabin Wu:** Resources, Data curation, Writing – review & editing. **Huaming Yu:** Visualization, Investigation. **Xiaoning Luan:** Validation. **Fupeng Wang:** Software. **Qingsheng Xue:** Supervision.

Declaration of Competing Interest

The authors declare that they have no known competing financial interests or personal relationships that could have appeared to influence the work reported in this paper.

Data availability

No data was used for the research described in the article.

Acknowledgement

This work was supported Natural Science Foundation of Shandong Province (ZR2021QD140, ZR2020QF097), Fundamental Research Funds for the Central Universities (202113038), National Natural

Science Foundation of China (U2006209, 41575023, 41906163, 42076183, 52001295), and Key Research and Development Program of Shandong Province (2020CXGC010706).

References

[1] C.A.J. Putman, B.G.D. Grooth, N.F.V. Hulst, J. Greve, A detailed analysis of the optical beam deflection technique for use in atomic force microscopy, J. Appl. Phys. 72 (1992) 6–12.

[2] J. Zhang, M.A. Itzler, H. Zbinden, J.W. Pan, Advances in InGaAs/InP single-photon detector systems for quantum communication, Light-Sci Appl 4 (2015) e286.

[3] G.A. Tyler, D.L. Fried, Image-position error associated with a quadrant detector, J. Opt. Soc. Am 72 (1982) 804–808.

[4] Y. Panduputra, T.W. Ng, A. Neild, M. Robinson, Intensity influence on Gaussian beam laser based measurements using quadrant photodiodes, Appl. Opt 149 (19) (2010) 3669–3675.

[5] D. Schutze, V. Muller, G. Heinzel, Precision absolute measurement and alignment of laser beam direction and position, Appl. Opt 53 (28) (2014) 6503–6507.

[6] D. Zheng, X. Wang, F. Tang, An improved method of angle measurement with a position sensitive detector, Chin. Opt. Lett 5 (7) (2007) 403–406.

[7] V.J. Yallapragada, G.L. Mulay, C.N. Rao, A.P. Ravishankar, V.G. Achanta, Direct measurement of the Goos-Hänchen shift using a scanning quadrant detector and a polarization maintaining fiber, Rev. Sci. Instreum 87 (2016), 103109.

[8] D. Li, S. Liu, Research on four-quadrant detector and its precise detection, Int. J. Digital Content Technol 5 (2011) 138–143.

[9] L.M. Manojlović, Quadrant photodetector sensitivity, Appl. Opt 50 (20) (2011) 3461–3469.

[10] M. Toyoda, K. Araki, Y. Suzuki, Measurement of the characteristics of a quadrant avalanche photodiode and its application to a laser tracking system, Opt. Eng. 41 (1) (2002) 145–149.

[11] A. Mäkynen, "Position-sensitive devices and sensor systems for optical tracking and displacement sensing applications, Department of Electrical Engineering," Oulu University, Oulu, Finland, 2000 (Ph.D. thesis, October 2000).

[12] L. Zhang, Y. Yang, W. Xia, X. Zhu, W. Chen, Y. Lu, Linearity of quadrant avalanche photodiode in laser tracking system, Chin. Opt. Lett. 7 (8) (2009) 728–731.

[13] K.B. Fielhauer, B.G. Boone, J.R. Bruzzi, B.E. Kluga, J.R. Connelly, M.M. Bierbaum, J.J. Gorman, N.G. Dagalakis, Comparison of macro-tip/tilt and mesoscale position beam steering transducers for free-space optical communications using a quadrant photodiode sensor, Proc. SPIE 5160 (2003) 192–203.

[14] E. Akkal, Control actuation systems and seeker units of an air-to-surface guided munition, Middle East Technical University," (Master's thesis (2003).

[15] V. Garbin, G. Volpe, E. Ferrari, et al., Mie scattering distinguishes the topological charge of an optical vortex: a homage to Gustav Mie, New J. Phys. 11 (1) (2009).

[16] F. Gittes, C.F. Schmidt, Interference model for back-focal-plane displacement detection in optical tweezers, Opt. Lett 23 (1) (1998) 7–9.

[17] J. Zhang, W. Zhou, C. Mao, et al., A calibration and correction method for the measurement system based on four-quadrant detector, Optik 204 (2020), 164226.

[18] J. Narag, N. Hermosa, Response of quadrant detectors to structured beams via convolution integrals, JOSA A 34 (7) (2017) 1212–1216.

[19] S. Cui, Y.C. Soh, Linearity Indices and Linearity Improvement of 2-D Tetralateral Position-Sensitive Detector, IEEE Trans. Electron Devices 57 (2010) 2310–2316.

[20] S. Cui, Y.C. Soh, Analysis and improvement of Laguerre-Gaussian beam position estimation using quadrant detectors, Opt. Lett. 36 (2011) 1692–1694.

[21] W. Fu, S. Chen, J. Guan, Z. Zhang, H. Wu, D.F. Wang, A Virtual-Movement Scheme for Eliminating Spot-Positioning Errors Applicable to Quadrant Detectors, IEEE Trans. Instrum. Meas. 70 (2021) 1–11.

[22] Q. Li, J. Wu, Y. Chen, J. Wang, S. Gao, Z. Wu, A New Response Approximation Model of the Quadrant Detector Using the Optimized BP Neural Network, IEEE Sens. J. 20 (8) (2020) 4345–4352.

[23] X. Wang, X. Su, G. Liu, et al., Method to Improve the Detection Accuracy of Quadrant Detector Based on Neural Network, Photon. Technol. Lett. IEEE 33 (22) (2021) 1254–1257.

[24] A. Salmanpour, S.h. Mohammad Nejad, The Performance Improvement of the Target Position Determining System in Laser Tracking Based on 4Q Detector using Neural Network, Int. J. Electron. Commun. Eng. 5 (8) (2011).

[25] M. Chen, Y. Yang, X. Jia, H. Gao, Investigation of positioning algorithm and method for increasing the linear measurement range for four-quadrant detector, Optik 124 (24) (2013) 6806–6809.

[26] Q. Vo, X. Zhang, F. Fang, Extended the linear measurement range of four-quadrant detector by using modified polynomial fitting algorithm in micro-displacement measuring system, Opt. Laser Technol 112 (2019) 332–338.

[27] L.P. Salles, D.W.L. Monteiro, Designing the response of an optical quad-cell as position-sensitive detector, IEEE Sens. J 10 (2) (2010) 286–293.

[28] D. W. L. Monteiro, "CMOS-based integrated wavefront sensor," Ph.D. dissertation, Dept. Information Technology and Systems, TU Delft, Delft, Nederland (2002).

[29] X. Jing, H. Cheng, C. Xu, Y. Feng, Method to measure the position offset of multiple light spots in a distributed aperture laser angle measurement system, Appl. Opt 23 (1) (2017) 1740–1747.

[30] Q. Li , J. Wu, Y. Chen, J. Wang, S. G and Z. Wu, "High Precision Position Measurement Method for Laguerre-Gaussian Beams Using a Quadrant Detector," Sensors 18(11), 4007 (2018).

[31] J. Wu, B. Zhao, Z. Wu, Improved measurement accuracy of the spot position on an InGaAs quadrant detector by introducing Boltzmann function, ICOM 183–185 (2015).

[32] J. Wu, Y. Chen, S. Gao, Y. Li, Z. Wu, Improved measurement accuracy of spot position on an In GaAs quadrant detector, Appl. Opt 154 (27) (2015) 8049–8054.

[33] E.J. Lee, Y. Park, C.S. Kim, T. Kouh, Detection sensitivity of the optical beam deflection method characterized with the optical spot size on the detector, Curr. Appl. Phys. 10 (2010) 834–837.

[34] B. Schmidt, R. Ross, Position-sensitive photodetectors made with standard silicon-planar technology, Sens. Actuators 4 (1983) 439–446.

[35] X. Ma, C. Rao, K. Wei, Y. Guo, X. Rao, Error analysis of the decrosstalk algorithm for the multianode-PMT-based quadrant tracking sensor, Opt. Express 20 (28) (2012) 29185–29195.